Image Reconstruction of Defects in Metallic Plates Using a Multifrequency Detector System and a Discrete Geometric Approach

E. Cardelli[1,2,3], A. Faba[1,2,3], R. Specogna[4], and F. Trevisan[4]

[1]Department of Industrial Engineering, Perugia University, 06124 Perugia, Italy
[2]Polo Scientifico Didattico di Terni, 05100 Terni, Italy
[3]Center for Electric and Magnetic Applied Research, 06124 Perugia, Italy
[4]Department of Ingegneria Elettrica, University of Udine, I-33100 Udine, Italy

We present an inversion procedure for the image reconstruction of defects in metallic plates, using a multifrequency eddy-current system. The solution of the eddy-current forward problem is achieved by means of a discrete geometric approach, while the inverse problem is resolved with an iterative linearization algorithm based on sensitivity data. In particular, we propose a suitable measurement point on the region under test using a probe coil exited by means a multifrequency signal, in order to improve the amount of usable data and the accuracy of the inverse procedure.

Index Terms—**Discrete geometric approach, inverse problems, multifrequency eddy currents, sensitivity analysis.**

I. Introduction

EDDY-current inspections is one of the most interesting approaches in electromagnetic nondestructive evaluation of metallic materials. The presence of a defect produces an impedance variation of the probe coil and, therefore, in the voltage or current at the coil leads, that we can use to locate the defect and also to estimate its shape and depth, so that we can verify the integrity of the plate [1]–[4]. To this aim, we use 3-D image reconstruction algorithms based on an inversion procedure elaborating experimental data together with solutions of proper forward problems. The results presented in this paper have been obtained using simulated data instead of the experimental ones. The direct model is based on a discrete geometric approach for electromagnetic field, by means of integral quantities associated with the oriented geometric elements of a pair of interlocked cell complexes [5]–[13].

II. Multifrequencies Detector System

In general, the 3-D image reconstruction of defects in a material has been derived by means of suitable detection systems consisting of several probe coils [14], [15]. Indeed the multiprobe coil systems provide many data to be considered in the sensitivity analysis. Nevertheless, they cannot be enough to assure an accurate resolution of the inverse problem which remains highly "ill-posed." Moreover, in most of practical applications, only a finite portion of the sample under inspection is available to be tested. In this case, increasing the number of probe coil positions could lead to redundant data that are useless in the inversion procedure. Therefore, in this work, we present a multifrequency excitation for the probe coil, in order to reduce the "ill-posed" characteristic of the problem and to improve the inversion procedure, in terms of capability to distinguish the depth of the defect. In particular, in this paper, we show some results obtained using two values of frequencies 500 Hz and 1 kHz, associated with two different depth of inspection, and with 13 different positions of the probe coil on the metallic plate. For each frequency, we impose a unitary excitation current and so we calculate the variation of the voltage at the probe coil leads.

III. Forward Problem

We introduce in the domain of interest (containing the conductive region V_c) a pair of interlocked cell complexes: the primal K, based on simplexes, and its barycentric dual $\tilde{K}$, [5]–[8]. The mutual interconnections between the cell complex $K, \tilde{K}$ are described by the incidence matrices: $\mathbf{G}$ between edges and nodes, $\mathbf{C}$ between faces and edges, and $\mathbf{D}$ between volumes and faces. The matrices $\tilde{\mathbf{G}} = \mathbf{D}^T, \tilde{\mathbf{C}} = \mathbf{C}^T$ and $\tilde{\mathbf{D}} = -\mathbf{G}^T$ describe the mutual interconnections of $\tilde{K}$. The arrays of degree of freedoms can be associated univocally to the elements of K or $\tilde{K}$. We have that $\mathbf{U}$ is the array of voltages on primal edges, $\mathbf{\Phi}$ is the array of fluxes on primal faces, $\mathbf{F}$ is the array of magnetic voltages on dual edges and $\mathbf{I}$ is the array of currents on dual faces. The physical laws of the eddy-current problem, can be written *exactly*, as follows: $\mathbf{D\Phi} = 0$ (Gauss' law); $\tilde{\mathbf{C}}\mathbf{F} = \mathbf{I}$ (Ampère's law); $\mathbf{CU} = -i\omega\mathbf{\Phi}$ (Faraday's law); and $\tilde{\mathbf{D}}\mathbf{I} = 0$ (continuity law). In addition, the discrete magnetic and Ohm's constitutive equations are, respectively, $\mathbf{F} = \boldsymbol{\nu}\mathbf{\Phi}, \mathbf{I} = \boldsymbol{\sigma}\mathbf{U}$, where $\boldsymbol{\nu}, \boldsymbol{\sigma}$ are two square matrices ($F \times F$ and $E \times E$, respectively). These matrices can be derived in a geometric way as described in [8]–[13]. To solve the discrete eddy-current problem [10], [11], we search for an array $\boldsymbol{\chi}$ of scalar potential values on primal nodes of the conducting region

Digital Object Identifier 10.1109/TMAG.2007.892525

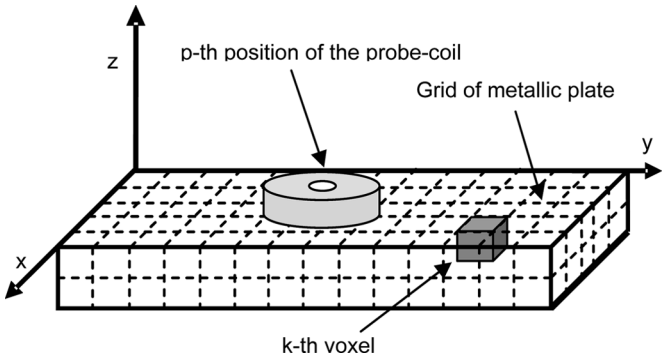

Fig. 1. Detector system configuration.

TABLE I
DIMENSIONS OF THE PROBE COIL

Parameter	Values
Inner Radius	1.5 mm
Outer Radius	6 mm
Heigth	7 mm
Number of Turns	400
Lift-Off	0.5 mm

and for array $\mathbf{a}$ of circulations of the magnetic vector potential on primal edges. In this way, Gauss' law and Faraday's law are satisfied identically when we write, respectively, $\mathbf{\Phi} = \mathbf{Ca}$ and $\mathbf{U} = -i\omega(\mathbf{a} + \mathbf{G}\boldsymbol{\chi})$. A first set of equations, relative to the primal edges, is derived by substituting in Ampère's law the discrete magnetic constitutive equation, where the array of fluxes is expressed in terms of $\mathbf{a}$. We obtain $\tilde{\mathbf{C}}\boldsymbol{\nu}\mathbf{Ca} = \mathbf{I}$, where $\mathbf{I}$ is null in nonconducting regions. A second set of equations can be written, associated with primal edges in the conducting region, by substituting in Ohm's constitutive equation, Faraday's law, and the previous relation, obtaining $[\tilde{\mathbf{C}}\boldsymbol{\nu}\mathbf{C} + i\omega\boldsymbol{\sigma}]\mathbf{a} + i\omega\boldsymbol{\sigma}\mathbf{G}\boldsymbol{\chi} = \mathbf{0}$. The last set of equations is written for the primal nodes in the conducting region, by substituting the Ohm constitutive equation and Faraday's law in the continuity equation. We obtain $i\omega\tilde{\mathbf{D}}\sigma\mathbf{a} + i\omega\tilde{\mathbf{D}}\sigma\mathbf{G}\chi = \mathbf{0}$.

As a result of the linearity of media, we have expressed the array $\mathbf{a}$ as the sum of the array $\mathbf{a}_s$ of circulations of the contribution to the magnetic vector potential produced by the source currents and the array $\mathbf{a}_r$ of circulations of the contribution to the magnetic vector potential due to the eddy-currents in the conducting region. Then we precomputed the array $\mathbf{a}_s$ by means of an integral representation of the source currents. In this way, we can remove the source currents $\mathbf{I}$ from the right-hand side of the final system.

IV. INVERSION PROCEDURE

We have considered a plate of aluminium (conductivity: 37.7 10^6 S/m), with a thickness equal to 4 mm and indefinite dimensions along the other two directions. We focalize our attention on a square region of the plate of 3 cm × 3 cm, divided into a regular grid of cubes named "voxels," whose edge is equal to 2 mm and which represents the basic volumetric amount. So, we have a total number of 450 voxels, and our aim is to estimate the value of electrical conductivity "σ_k" at each voxel (see Fig. 1). We consider a probe coil having the dimensions shown in Table I.

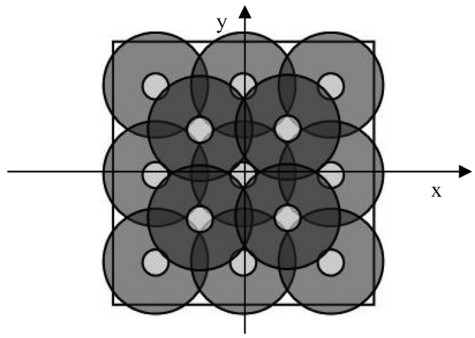

Fig. 2. Probe coil positions over the area under test.

TABLE II
POSITIONS OF THE PROBE COIL ON THE AREA UNDER TEST

Position	x [mm]	y [mm]	Position	x [mm]	y [mm]
1	-10	10	8	10	0
2	0	10	9	5	-5
3	10	10	10	-5	-5
4	-5	5	11	-10	-10
5	5	5	12	0	-10
6	-10	0	13	-10	-10
7	0	0			

This probe coil respects technological limits of coil realization with commercial winding machines and at the same time is the most proportioned in terms of inner radius (outer radius) height. In our procedure, we move the probe coil in 13 different positions, arranged over the plate to optimize the tradeoff between minor number of positions and greater recovering of the voxel region. Setting the center of the voxel region (3 cm × 3 cm) described previously as the origin (0, 0) of a coordinate system (see Fig. 2), the positions of the center of the coil are shown in Table II.

For each probe coil position "p," and for each frequencies considered "i," the voltage output is calculated by means of a numerical direct model, in function of the conductivity map

$$V_{p,i} = f(\sigma_1, \sigma_2, \sigma_3, \ldots, \sigma_k, \ldots). \tag{1}$$

At the same time each element of the sensitivity matrix is defined as

$$S_{k,p,i} = \frac{\partial V_{p,i}}{\partial \sigma_k}. \tag{2}$$

In this way, each row of the sensitivity matrix represents a configuration of measure, i.e., a fixed position of the probe coil at a fixed frequency, while each column represents a voxel of the plate. It was found that for the present eddy-currents problem the derivative of the probe coil voltage with respect to the voxel conductivity can be expressed in the following compact expression [14]:

$$S_{k,p,i} = -\frac{1}{I_{p,i}^2} \int_{\Omega_k} |\vec{E}_{p,i}(\vec{r})|^2 \, d\vec{r} \tag{3}$$

where $I_{p,i}$ is the current in the probe coil "p" at the frequency "i," Ω_k is the volume of the kth voxel and $\vec{E}_{p,i}$ is the electric field in the element volume generated from the probe coil in the

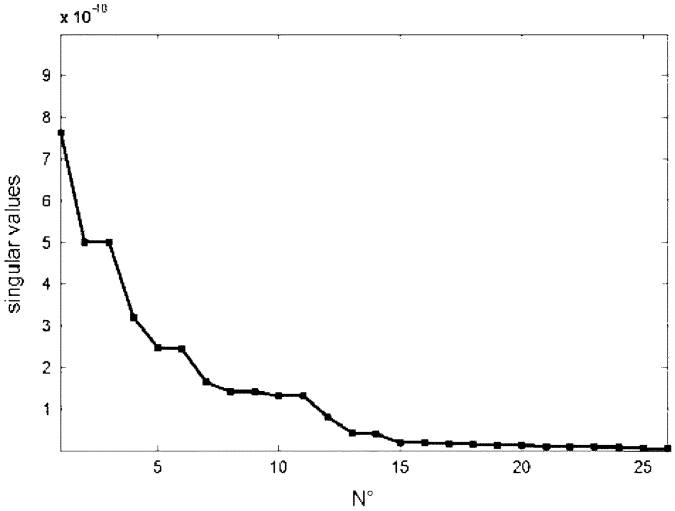

Fig. 3. Singular values of the sensitivity matrix (linear scale).

position "p" at the frequency "i." In this work, the excitation current is assumed unitary. The sensitivity matrix is calculated solving the forward problem, then the distribution of the electric conductivity is iteratively upgraded using a procedure of minimization of the differences between the real values of voltages at the probe coil leads and the computed ones. In general, the real values of voltages can be obtained from a measurements, but at the moment, in this work, we calculate these values by means of direct problem simulations, considering the real defect as a well defined number of voxels with imposed conductivity equal to zero. We have matured some experience about the use of noisy computed data instead of experimental ones; also, in this case, the inversion procedure presented here is efficient. The iterative process start with a uniform distribution of conductivity $\vec{\sigma}$, i.e., with a plate without defects, and at each iteration the variation of $\vec{\sigma}$ for each voxel is calculated as follows:

$$\Delta\vec{\sigma}_{n+1} = \hat{\mathbf{S}}_n^{\mathrm{T}} \left(\hat{\mathbf{S}}_n \hat{\mathbf{S}}_n^{\mathrm{T}}\right)^{-1} (\vec{\mathbf{V}} - f(\vec{\sigma}_n)) \tag{4}$$

where "n" is the number of iteration, $\hat{\mathbf{S}}$ is the sensitivity matrix and $\vec{V}$ is the vector of the voltage data obtained from the real distribution of the electric conductivity.

Moreover, we have obtained a progressive reduction of the variation of conductivity calculated using (4), so that the convergence of the iterative process is guaranteed avoiding too large increments. Therefore, the (4) can be expressed as follows:

$$\Delta\vec{\sigma}_{n+1} = \alpha_1 \cdot \hat{\mathbf{S}}_n^{\mathrm{T}} \left(\hat{\mathbf{S}}_n \hat{\mathbf{S}}_n^{\mathrm{T}}\right)^{-1} [(\vec{\mathbf{V}} - f(\vec{\sigma}_n)) - \alpha_2 \cdot \hat{\mathbf{S}}_n \Delta\vec{\sigma}_n] \tag{5}$$

where α_1 is the reduction factor, which value diminish as the iterations go on. Moreover, we introduce in (5) a penalty term to minimize the norm of the variation of conductivity at each step. This penalty is the product of the sensitivity matrix and the variation of $\vec{\sigma}$ calculated at the previous iteration. However, this term is reduced of a factor α_2, for example, equal to 50%. In this way, we impose that the variation at the step $n+1$ must not be too great referred to the variation at the previous step n. We introduce a damping factor chosen frequency dependent and determined to optimize the resolution in the z-direction (see Fig. 1). In particular, we operate a normalization of the singular values of the sensitivity matrix, considering the different values of frequencies. After this normalization, we obtain the diagrams of singular values in Fig. 3, referred to the first iteration. In order to improve the convergence of the solution process, we also correct back to aluminium the computed values of conductivity greater than the value peculiar to aluminum, and back to zero the values minor of zero. The iterative procedure is terminated when the difference between the measured voltage on the probe coils and the voltage simulated at the current step has the global minimum.

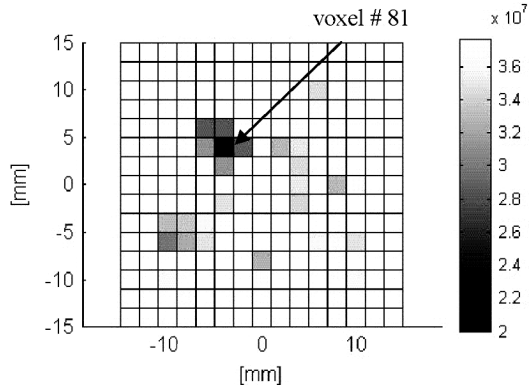

Fig. 4. Results about the inversion procedure for the test 1. Conductivity distribution on the first layer of the metallic plate obtained at the iteration $n°5$ (color bar S/m).

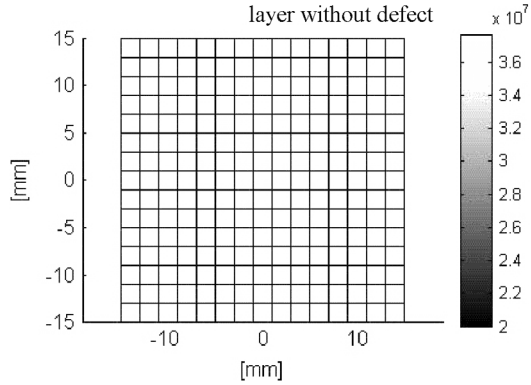

Fig. 5. Results about the inversion procedure for the test 1. Conductivity distribution on the second layer of the metallic plate (2 mm of depth), obtained at the iteration $n°5$ (color bar S/m).

V. Results

In this paper, we present two tests, in the first, there is only one defect on the plate, in the second, there are two defects at two different depth. For the first test, we have considered a defect corresponding to the voxel number 81, i.e., a cube-shaped defect in the first layer of voxel, while the second layer is considered without any defects. Starting from an uniform configuration of $\vec{\sigma}$ and proceeding with the iterations, after five steps, we have obtained the map of $\vec{\sigma}$ reported in Fig. 4 for the first layer and in Fig. 5 for the second layer. The position of the defect in the metallic plate is determined with a good accuracy. For the second test, we have considered two defects arranged on the two different layers, exactly on voxel number 65 (first layer at the plate surface) and voxel number 386 (second layer at 2 mm of depth respect to the plate surface). In this case, the results of the inversion procedure are reported in Figs. 6 and 7. We have

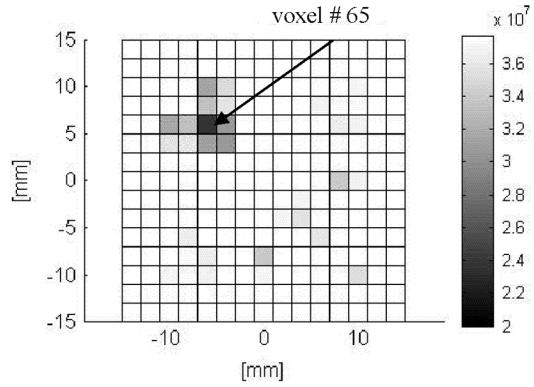

Fig. 6. Results about the inversion procedure for the test 2. Conductivity distribution on the first layer of the metallic plate obtained at the iteration $n°10$ (color bar S/m).

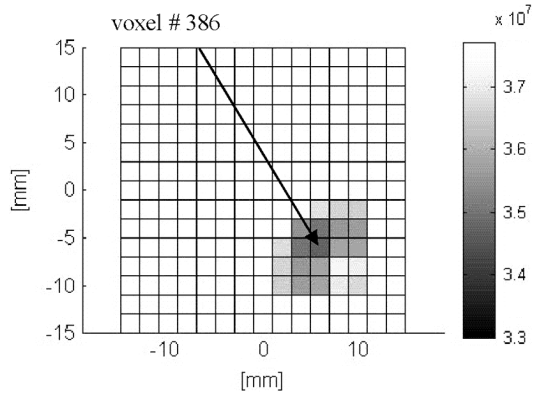

Fig. 7. Results about the inversion procedure for the test 2. Conductivity distribution on the second layer of the metallic plate (2 mm of depth), obtained at the iteration $n°10$ (color bar S/m).

a clear image of the defect in the first layer, while the defect on the second layer is detected with minor accuracy.

VI. Conclusion

A 3-D imaging inversion algorithm based on multifrequency eddy currents nondestructive inspection is presented. The procedure exploits a forward problem solution achieved by means discrete geometric approach for electromagnetic field and an inversion procedure based on sensitivity linearization.

Preliminary results seem to indicate that multifrequency analysis (500 Hz with 3.7 mm of skin depth, 1 kHz with 2.6 mm of skin depth) improves the stability of the inverse procedure and provides good results for the 3-D reconstruction of a defect also when it is located at different depth in the metallic plate.

Acknowledgment

This work was supported by the Italian Ministry of Education-Scientific Program PRIN 2004–2006 Application of Methods of Electromagnetic Diagnostic (AMDE).

References

[1] E. Cardelli and A. Faba, "FEM analysis of thin cracks in metallic plates," *Int. J. Appl. Electromagn. Mech.*, vol. 19, pp. 503–507, 2004.
[2] E. Cardelli and A. Faba, "About the sensibility of eddy current nondestructive testing," in *Proc. XII Int. Symp. Theoretical Electr. Eng. (ISTET)*, 2003, pp. 345–348.
[3] E. Cardelli, A. Faba, and M. Tomassini, "FEM time domain analysis for the detection of depth and thickness of cylindrical defects in metallic plates," *IEEE Trans. Magn.*, vol. 41, no. 5, pp. 1616–1619, May 2005.
[4] E. Cardelli, A. Faba, R. Specogna, A. Tamburino, F. Trevisan, and S. Ventre, "Analysis methodologies and experimental benchmarks for eddy current testing," *IEEE Trans. Magn.*, vol. 41, no. 5, pp. 1380–1383, May 2005.
[5] A. Bossavit, "How weak is the weak solution in finite element methods?," *IEEE Trans. Magn.*, vol. 34, no. 5, pp. 2429–2432, May 1998.
[6] E. Tonti, "Algebraic topology and computational electromagnetism," in *Proc. 4th Int. Workshop Electric Magn. Fields*, 1988, pp. 284–294.
[7] E. Tonti, "Finite formulation of electromagnetic field," *IEEE Trans. Magn.*, vol. 38, no. 2, pp. 333–336, Mar. 2002.
[8] A. Bossavit and L. Kettunen, "Yee-like schemes on staggered cellular grids: A synthesis between FIT and FEM approaches," *IEEE Trans. Magn.*, vol. 36, no. 4, pp. 861–867, Jul. 2000.
[9] R. Specogna and F. Trevisan, "Discrete constitutive equations in $A-\chi$ geometric eddy-currents formulation," *IEEE Trans. Magn.*, vol. 41, no. 4, pp. 1259–1263, Apr. 2005.
[10] F. Trevisan, "3-D eddy current analysis with the cell method for DE problems," *IEEE Trans. Magn.*, vol. 40, no. 2, pp. 1314–1317, Mar. 2004.
[11] F. Trevisan and L. Kettunen, "Geometric interpretation of finite-dimensional eddy-current formulations," *Int. J. Numer. Methods Eng.*, vol. 67, no. 13, pp. 1888–1908, 2007.
[12] L. Codecasa and F. Trevisan, "Piecewise uniform bases and energetic approach for discrete constitutive matrices in electromagnetic problems," *Int. J. Numer. Methods Eng.*, vol. 65, no. 4, pp. 548–565, 2007.
[13] F. Trevisan and L. Kettunen, "Geometric interpretation of discrete approaches to solving magnetostatic problems," *IEEE Trans. Magn.*, vol. 40, no. 2, pp. 361–365, Mar. 2004.
[14] D. N. Dyck and D. A. Lowther, "A method of computing the sensitivity of electromagnetic quantities to change in materials and sources," *IEEE Trans. Magn.*, vol. 30, no. 5, pp. 3415–3418, Sep. 1994.
[15] M. Soleimani and W. R. B. Lionheart, "Image reconstruction in three-dimensional magnetostatic permeability tomography," *IEEE Trans. Magn.*, vol. 41, no. 4, pp. 1274–1279, Apr. 2005.

Manuscript received April 24, 2006 (e-mail: faba@unipg.it).